

Insensitivity of the elastic proton-nucleus reaction to the neutron radius of ^{208}Pb

J. Piekarewicz^{1,*} and S.P. Weppner^{2,†}

¹*Department of Physics, Florida State University, Tallahassee FL 32306*

²*Natural Sciences, Eckerd College, St. Petersburg FL 33711*

(Dated: November 14, 2018)

Abstract

The sensitivity—or rather insensitivity—of the elastic proton-nucleus reaction to the neutron radius of ^{208}Pb is investigated using a non-relativistic impulse-approximation approach. The energy region ($T_{\text{lab}} = 500$ MeV and $T_{\text{lab}} = 800$ MeV) is selected so that the impulse approximation may be safely assumed. Therefore, only free nucleon-nucleon scattering data are used as input for the optical potential. Further, the optical potential includes proton and neutron ground-state densities that are generated from accurately-calibrated models. Even so, these models yield a wide range of values (from 0.13 fm to 0.28 fm) for the poorly known neutron skin thickness in ^{208}Pb . An excellent description of the experimental cross section is obtained with all neutron densities. We have invoked analytic insights developed within the eikonal approximation to understand the insensitivity of the differential cross section to the various neutron densities. As the diffractive oscillations of the cross sections are controlled by the matter radius of the nucleus, the large spread in the neutron skin among the various models gets diluted into a mere 1.5% difference in the matter radius. This renders ineffective the elastic reaction as a precision tool for the measurement of neutron radii.

PACS numbers: 21.10.Gv, 25.40.Cm, 24.10.Ht

*Electronic address: jorgep@csit.fsu.edu

†Electronic address: weppnesp@eckerd.edu

I. INTRODUCTION

The neutron radius of a heavy nucleus—such as ^{208}Pb —is a fundamental nuclear structure quantity that remains elusive. This is in striking contrast to the proton radius that is known with exquisite accuracy for a variety of nuclei throughout the periodic table [1]. For example, the charge radius of ^{208}Pb is known with a 0.01% accuracy ($R_{\text{ch}} = 5.5013(7)$ fm). The origin of the mismatch in our knowledge of such similar quantities is the availability for over half a century of high-quality electron beams to accurately map the nuclear charge distribution [2]. Instead, mapping the neutron distribution has relied on strongly-interacting probes that suffer from controversial uncertainties in the reaction mechanism [3, 4], thereby hindering the extraction of such fundamental observable.

Parity violating electron nucleus scattering offers an attractive alternative to the hadronic program. The Parity Radius Experiment (PREX) at the Jefferson Laboratory aims to measure the neutron radius of ^{208}Pb accurately (to within 0.05 fm) and model independently via parity-violating electron scattering [5, 6]. Parity violation is sensitive to the neutron density because the Z^0 boson couples primarily to neutrons, as its vector coupling to the proton is suppressed by the weak mixing angle ($1 - 4 \sin^2 \theta_W \approx 0.076$). The parity-violating asymmetry, while small, can be interpreted with as much confidence as electromagnetic scattering experiments. PREX should provide a unique observational constraint on the thickness of the neutron skin of a heavy nucleus.

While measuring the neutron radius of a heavy nucleus should be reason enough to endorse the experiment, the search for this fundamental quantity has been recently stimulated by theoretical evidence that a precise measurement of the neutron radius in ^{208}Pb could place an important new constraint on the neutron-matter equation of state [7]. Moreover, it has been also suggested that an accurate measurement of the neutron radius in ^{208}Pb will impact strongly on a host of neutron-star observables, such as on their structure, composition, and cooling mechanism [8, 9, 10, 11, 12]. Prompted by these new developments, several new analysis of proton-nucleus elastic scattering have been reported [13, 14, 15].

In Ref. [13] an analysis of both proton-nucleus (pA) and neutron-nucleus (nA) elastic scattering suggested a value for the neutron skin of ^{208}Pb —defined as the difference between its neutron (R_n) and proton (R_p) root-mean-square radii—of $\Delta R \equiv R_n - R_p \sim 0.17$ fm. The model employs a sophisticated “g-folding” optical potential [16] that incorporates proton densities constrained from electron scattering and several model neutron densities. The neutron densities employed were generated from either accurately calibrated Skyrme parameterizations or from simple harmonic-oscillator models. While the harmonic-oscillator parameters were adjusted to reproduce some average properties of ^{208}Pb , the Skyrme model parameters were generated from a bona fide fit to a large body of ground-state data. Calculations were performed at laboratory kinetic energies of $T_{\text{lab}} = 40, 65,$ and 200 MeV for ^{40}Ca and ^{208}Pb . While the proton- ^{208}Pb differential cross section at $T_{\text{lab}} = 200$ MeV shows clear differences at large scattering angles between the Skyrme and harmonic-oscillator densities (with the former being clearly favored) the differences among the accurately calibrated sets appears to be marginal.

The value of $\Delta R \sim 0.17$ fm proposed in Ref. [13] is consistent with a very recent analysis that suggests a neutron skin in the range $\Delta R \sim 0.13$ – 0.17 fm [15]. While this $T_{\text{lab}} = 121$ MeV calculation is also based on a g-folding approach, it employs, in addition to the SKM* interaction responsible for the $\Delta R \sim 0.17$ fm value, a neutron density generated in a random-phase-approximation (RPA) that yields the smaller value of 0.13 fm for the neutron skin.

Finally, the global analysis of medium-energy ($T_{\text{lab}} = 500\text{--}1040$ MeV) pA elastic-scattering data of Ref. [14] reports a skin thickness in ^{208}Pb of $\Delta R \sim 0.083\text{--}0.111$ fm, slightly smaller than the previous two analyzes. The extraction of neutron densities, not only for the case of ^{208}Pb but also for ^{40}Ca and ^{48}Ca , is based on a global Dirac-phenomenological approach. The merit of the approach is (at least) twofold. First, the analysis is limited to an energy region that is well described by the impulse approximation. Thus, the approach relies on existent experimental on-shell nucleon-nucleon (NN) data. This avoids modeling important and often complicated medium modifications to the NN interaction. Second, the various parameters characterizing the neutron density are determined from a global fit to a large body of scattering observables (differential cross sections and spin observables) at a variety of projectile energies. What emerges from this global fit is the optimal set of parameters characterizing the neutron densities. In stark contrast to an earlier analysis by Ray [4], this approach produces energy-independent neutron radii.

Nuclear giant resonances have also been used recently to place some constraints on the neutron radius of ^{208}Pb [17]. In order to simultaneously reproduce the isovector giant dipole resonance in ^{208}Pb as well as the isoscalar giant-monopole resonance in both ^{208}Pb and ^{90}Zr , a neutron skin in ^{208}Pb of $\Delta R \lesssim 0.21$ fm was required [18]. While this value is significantly lower than the ones obtained with earlier relativistic parameter sets [19], it remains higher relative to the values obtained from the NA scattering analyzes described above.

In our effort to test the sensitivity of nucleon-nucleus scattering to the neutron radius of ^{208}Pb , we have modified the isovector parameters of the model so that the neutron radius of ^{208}Pb may be adjusted—while maintaining the proton radius fixed at its experimental value. Our numerical calculations of the differential cross section are in very good agreement with experimental data and show no clear distinction among the various nuclear-structure models. To elucidate the insensitivity of the differential cross section to the neutron density, we have invoked analytic insights developed within the eikonal approximation [20, 21]. Such analyzes reveal that while the filling of the diffractive oscillations germane to the differential cross section are determined by the underlying dynamics, the diffractive oscillations and exponential falloff of the cross sections are dominated by the nuclear geometry—with the radius controlling the oscillations and the diffuseness parameter the exponential falloff. Thus the nuclear radius leaves its imprint in the diffractive oscillations of the differential cross section. However, at the medium energies considered here, the cross section is dominated by the isoscalar (or matter) density. Hence, the factor of two difference in the model dependence of the neutron skin translates into a minute 1.5% difference in the matter radius that can not be resolved. We conclude that the elastic reaction may not serve as a precision tool for the measurement of neutron radii.

The manuscript has been organized as follows. In Sec. II we present the formalism employed in the calculations. This section includes a subsection that introduces the various nuclear-structure models employed to generate proton and neutron densities. An additional subsection discusses how these nuclear densities are incorporated into the various treatments of the optical potential. In Sec. III we present results for the differential cross section for the scattering of $T_{\text{lab}} = 500$ and 800 MeV protons from ^{208}Pb . Finally, we offer our conclusions in Sec. IV.

II. FORMALISM

This section starts with a discussion of the nuclear-structure model employed in the calculations. In particular, it includes four parameterizations that yield neutron skins in ^{208}Pb ranging from $\Delta R=0.13$ fm to $\Delta R=0.28$ fm, while keeping the charge radius fixed at its experimental value. Next, we discuss briefly how these various densities get incorporated into the treatment of the optical potential.

A. Nuclear-Structure Models

The nuclear densities employed in this contribution are derived from an effective field theoretical model that provides an accurate description of the ground-state properties of finite nuclei. The model is based on an interacting Lagrangian that has the following form [9, 10, 22]:

$$\begin{aligned} \mathcal{L}_{\text{int}} = & \bar{\psi} \left[g_s \phi - \left(g_v V_\mu + \frac{g_\rho}{2} \boldsymbol{\tau} \cdot \mathbf{b}_\mu + \frac{e}{2} (1 + \tau_3) A_\mu \right) \gamma^\mu \right] \psi \\ & - \frac{\kappa}{3!} (g_s \phi)^3 - \frac{\lambda}{4!} (g_s \phi)^4 + \frac{\zeta}{4!} \left(g_v^2 V_\mu V^\mu \right)^2 + \Lambda_v \left(g_\rho^2 \mathbf{b}_\mu \cdot \mathbf{b}^\mu \right) \left(g_v^2 V_\mu V^\mu \right). \end{aligned} \quad (1)$$

The Lagrangian density includes Yukawa couplings of the nucleon field (ψ) to isoscalar scalar (ϕ) and vector (V^μ) meson fields. This “minimal” model—introduced by Walecka more than 30 years ago [23]—provides a natural explanation for the saturation of symmetric nuclear matter. To describe asymmetric matter the model was extended by Serot to the isovector sector by introducing an isovector-vector meson (\mathbf{b}^μ). Using these three meson fields—plus the photon—Horowitz and Serot performed the first mean-field calculations of the ground-state properties of finite nuclei [24]. Yet the model had to be supplemented by nonlinear scalar-meson interactions (κ and λ) to soften the equation of state of symmetric nuclear matter, thereby obtaining compression moduli consistent with experiment. The mixed isoscalar-isovector coupling (Λ_v) is used to modify the density dependence of the symmetry energy and thus tune the neutron radius of ^{208}Pb without affecting other ground-state observables [9, 10]. This freedom is exploited here to generate ground-state densities having neutron skins in the range of $\Delta R = 0.13 - 0.28$ fm. Finally, the quartic vector-meson coupling (ζ) impacts the high-density component of the equation of state and is therefore weakly sensitive to the ground-state properties of finite nuclei [22]. The existence of powerful new telescopes studying neutron stars at a variety of wavelengths will provide important constraints on the poorly-known high-density component of the equation of state.

The model parameters used to compute the ground-state densities are listed in Table I. Both NL3 [19] and FSUGold [18] are accurately calibrated models obtained from a fit to ground-state properties of finite nuclei. The remaining two sets, FSUGold4 and FSUGold5, are obtained from FSUGold by adjusting the isovector parameters of the model (g_ρ and Λ_v) as prescribed in Ref. [9, 10]. This simple prescription enables one to reduce the neutron skin in ^{208}Pb without affecting the properties of symmetric nuclear matter. Note, however, that a slight reduction of the sigma-meson mass is also necessary to maintain the charge radius of ^{208}Pb within a fraction of one percent of its experimental value. In summary, we have used accurately calibrated relativistic mean-field models to compute the ground-state densities of ^{208}Pb . As the neutron radius in ^{208}Pb is not tightly constrained by existent ground-state observables, a few of the parameters of the model are adjusted to produce a

Model	m_s	g_s^2	g_v^2	g_ρ^2	κ	λ	ζ	Λ_v
NL3	508.194	104.387	165.585	79.600	3.860	-0.016	0.000	0.000
FSUGold	491.500	112.200	204.547	138.470	1.420	+0.024	0.060	0.030
FSUGold4	491.000	112.200	204.547	182.622	1.420	+0.024	0.060	0.040
FSUGold5	490.250	112.200	204.547	268.103	1.420	+0.024	0.060	0.050

TABLE I: Model parameters used in the calculations. The parameter κ and the inverse scalar range m_s are given in MeV. The nucleon, omega, and rho masses are kept fixed at $M=939$ MeV, $m_\omega=782.5$ MeV, and $m_\rho=763$ MeV, respectively.

wide range of values for its nucleon skin, while maintaining the charge radius fixed at its experimental value (see Table II). For a fairly comprehensive recent review on how the ground-state densities are computed see Ref. [25]. The various neutron and proton densities generated by these models are displayed in Fig. 1.

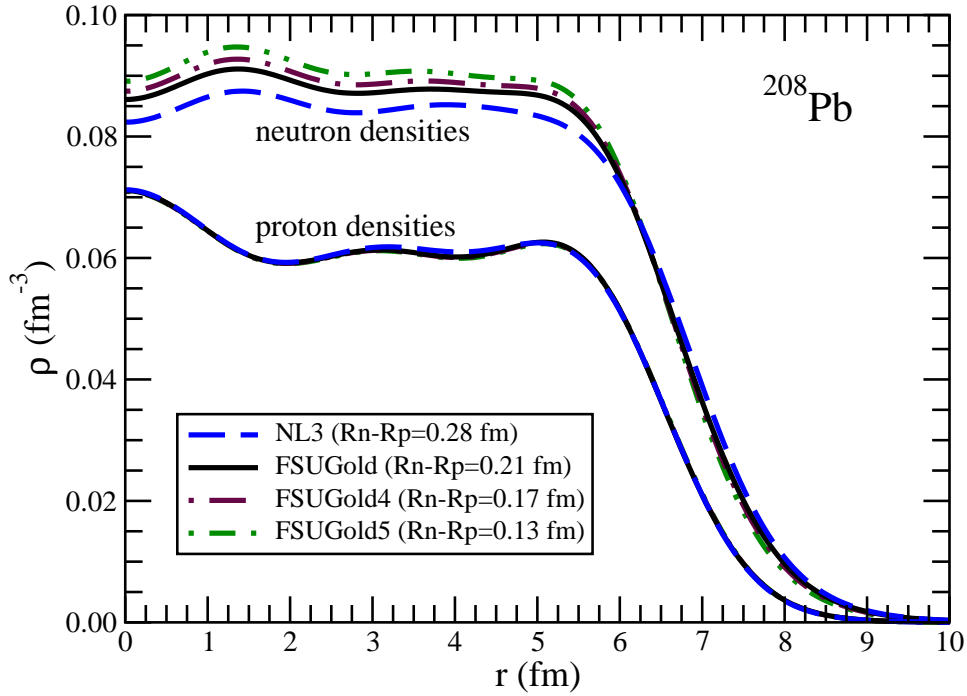


FIG. 1: Ground-state proton and neutron densities for ^{208}Pb predicted by the various models described in the text.

B. Scattering Formalism

Having generated ground-state densities that will serve as input for the optical potential, we present here a brief review of the scattering formalism employed in this work. For some excellent reviews of this very well developed field see, for example, Ref. [4] and references

Observable	Experiment	NL3	FSUGold	FSUGold4	FSUGold5
B/A (MeV)	7.87	7.88	7.89	8.10	8.42
R_{ch} (fm)	5.50	5.51	5.52	5.52	5.52
$R_n - R_p$ (fm)	—	0.28	0.21	0.17	0.13

TABLE II: Comparison between theory and experiment of the binding energy per nucleon and the charge radii of ^{208}Pb . Theoretical predictions are also displayed for the neutron skin.

contained therein.

Assuming invariance under rotation, parity, and time reversal, the model independent scattering amplitude for the elastic scattering of a nucleon from a spinless target may be written in terms of two amplitudes as follows:

$$\hat{\mathcal{F}}(\mathbf{k}, \mathbf{k}') = F_0(q, T_{\text{lab}}) + F_1(q, T_{\text{lab}}) \boldsymbol{\sigma} \cdot \hat{\mathbf{n}}, \quad (2)$$

where $\boldsymbol{\sigma}$ is the spin operator of the projectile and $\hat{\mathbf{n}} = \hat{\mathbf{q}} \times \hat{\mathbf{K}}$ is a unit vector perpendicular to the scattering plane. Here \mathbf{q} and \mathbf{K} denote the momentum transfer and average momentum of the collision in the center-of-momentum frame, respectively. That is,

$$\mathbf{q} = \mathbf{k} - \mathbf{k}' \quad \text{and} \quad \mathbf{K} = (\mathbf{k} + \mathbf{k}')/2. \quad (3)$$

Note that for the kinematical dependence of both, the spin-independent (F_0) and spin-dependent (F_1), amplitudes we have selected the kinetic energy of the projectile in the laboratory frame T_{lab} and the magnitude of the momentum transfer in the NA center-of-momentum frame $q = 2k \sin(\theta/2)$. Other choices are possible, yet the eikonal framework (discussed below) makes clear the advantage of using q .

As the NA scattering amplitude is written in terms of two independent complex functions, three independent observables are sufficient to fully characterize the reaction. It is customary to select the differential cross section ($d\sigma/d\Omega$), the analyzing power (A_y), and the spin-rotation function (Q) as the three independent observables. They are given by the following expressions:

$$\frac{d\sigma}{d\Omega} = |F_0|^2 + |F_1|^2, \quad (4a)$$

$$A_y = 2\text{Re} \left(\frac{F_0^* F_1}{|F_0|^2 + |F_1|^2} \right), \quad (4b)$$

$$Q = 2\text{Im} \left(\frac{F_0^* F_1}{|F_0|^2 + |F_1|^2} \right). \quad (4c)$$

As our main purpose is the extraction of the neutron radius of ^{208}Pb , we limit ourselves, as other have done before us, to study the differential cross section.

C. Non-relativistic Local KMT Optical Potential

The theoretical underpinning of most approximations to the elastic scattering of fast nucleons from nuclei is contained in the seminal work of Kerman, McManus, and Thaler (KMT) [26]. While it is not our intention to provide a comprehensive review of the formalism

(as an extensive literature is available) it is convenient to highlight a few aspects of the present approach.

To start, the nucleon-nucleus elastic scattering amplitude is written in terms of the “one-body” optical potential as follows:

$$\hat{\mathcal{F}}(\mathbf{k}, \mathbf{k}') = -\frac{m}{2\pi} \hat{\mathcal{T}}(\mathbf{k}, \mathbf{k}') = -\frac{m}{2\pi} \langle \mathbf{k}' | V_{\text{opt}} | \mathbf{k}+ \rangle, \quad (5)$$

where m is the nucleon mass and $|\mathbf{k}+\rangle$ denotes an “ $+i\epsilon$ ” nucleon distorted wave, namely, a plane wave of momentum \mathbf{k} in the infinite past. The on-shell microscopic KMT optical potential $V_{\text{opt}} = V_{\text{KMT}}$ for the scattering of a nucleon from a target nucleus with baryon number A is given by

$$V_{\text{KMT}}(\mathbf{q}) = \left(\frac{A-1}{A} \right) C(T_{\text{lab}}) \sum_{i=p,n} \hat{t}_{0i}(q, T_{\text{lab}}) \rho_i(q). \quad (6)$$

Note that for the scattering of medium-energy nucleons the impulse approximation is invoked, namely, the KMT optical potential contains the free NN t-matrix (\hat{t}_{0i}) between the projectile and the i -th target nucleon. Further, $\rho_i(q)$ denotes proton and neutron form factors obtained from the Fourier transform of their respective ground-state densities. Finally, the whole expression is multiplied by the following kinematical factor:

$$C(T_{\text{lab}}) \equiv \left(\frac{2}{E_p} \right)_{NN} \left(\frac{E_p E_t}{E_p + E_t} \right)_{NA}, \quad (7)$$

which preserves the unitarity of the nucleon-nucleon amplitude as it is transformed into the nucleon-nucleus CM frame [27]. Note that $E_p(E_t)$ is the projectile(target) energy evaluated in the center-of-momentum frame of either the NN or NA system. Although the formalism presented here is intrinsically non-relativistic, all kinematical variables are evaluated using relativistic kinematics. For nucleon scattering from a spin-saturated nucleus (such as ^{208}Pb) the only pieces of the elementary NN amplitude that contribute to the nucleon-nucleus elastic reaction are the central and spin-orbit pieces. That is, for the scattering from a spin-saturated nucleus one may write

$$\hat{f}_{0i}(q, T_{\text{lab}}) = -\frac{m}{2\pi} \hat{t}_{0i}(q, T_{\text{lab}}) \rightarrow A(q, T_{\text{lab}}) + iC(q, T_{\text{lab}}) \boldsymbol{\sigma} \cdot \hat{\mathbf{n}}, \quad (8)$$

where in the impulse approximation both of the “Wolfenstein” amplitudes (A and C) are directly inferred from free NN scattering data.

Having generated both nuclear form factors and the relevant components of the free NN t-matrix, one may now proceed to compute the elastic scattering cross section. This is implemented by solving the resulting Lippmann-Schwinger equation for the nucleon-nucleus t-matrix,

$$\hat{\mathcal{T}}_{KMT}(\mathbf{k}, \mathbf{k}') = \langle \mathbf{k}' | V_{\text{KMT}} | \mathbf{k}+ \rangle = \langle \mathbf{k}' | V_{\text{KMT}} | \mathbf{k} \rangle + \langle \mathbf{k}' | V_{\text{KMT}} G_0^{(+)} V_{\text{KMT}} | \mathbf{k}+ \rangle, \quad (9)$$

directly in momentum space through standard numerical techniques [27]. Note that $G_0^{(+)}$ denotes the free projectile propagator. It is important to mention that within the scope of the impulse approximation—and with ground-state form factors generated from an accurately calibrated parametrization—there are no adjustable parameters in the calculation.

D. Eikonal Approximation

The eikonal approximation provides a simple, physically illuminating picture of the scattering process at intermediate energies. In what follows we quote freely from the insightful review article by Amado [21]. In the eikonal approximation the elastic scattering amplitude is given in terms of an integral over impact parameter that effectively sums up the myriad of partial waves required at these intermediate energies. Moreover, at these energies the integrand oscillates rapidly making the scattering amplitude ideal for evaluation by the method of stationary phase. Through this analytic approach, the main features of the elastic NA reaction emerge in a clean and transparent way [20]. Indeed, the diffractive oscillations are controlled by the nuclear size, the exponential falloff by the diffuse nuclear surface, and the filling of the minima by Coulomb effects, the real part of the NN t-matrix, and spin effects. It is only this filling that depends on the underlying dynamics. Two of the main features of the diffractive cross section—oscillations and exponential decay—are completely determined by the nuclear geometry.

The spin-independent part of the scattering amplitude may be written in the eikonal approximation as an integral over impact parameter. That is,

$$F_0(q, T_{\text{lab}}) = \frac{iK}{2\pi} \int d^2b e^{i\mathbf{q}\cdot\mathbf{b}} (1 - e^{-\chi(\mathbf{b})}) , \quad (10)$$

where the profile function $\chi(\mathbf{b})$, still an operator in the spin space of the nucleon, is given by the following expression:

$$\chi(\mathbf{b}) = i\frac{m}{K} \int_{-\infty}^{\infty} dz V_{\text{opt}}(\mathbf{r}) , \quad (11)$$

where $V_{\text{opt}}(\mathbf{r})$ is the Fourier transform of the (assumed local) optical potential

$$V_{\text{opt}}(\mathbf{r}) = \int \frac{d^3q}{(2\pi)^3} e^{i\mathbf{q}\cdot\mathbf{r}} V_{\text{opt}}(\mathbf{q}) . \quad (12)$$

In the KMT approximation the optical potential $V_{\text{opt}}(\mathbf{q})$ is given by the form displayed in Eq. (6).

While in Sec. III results will be presented following the KMT formalism without any further approximation, the eikonal results include additional approximations so that contact may be established with the analytic approach developed by Amado and collaborators [20, 21]. One of these approximations emerges from comparing the range of the nuclear form factor relative to that of the central and spin-orbit pieces of the NN interaction (Eq. 8). For a spin-saturated nucleus, the long-range pion potential—which is strongly spin-dependent—does not contribute to leading order. This suggests that both the central and spin-orbit pieces of the NN interaction are short ranged. Alternatively, in a meson-exchange picture, only multiple-pion exchanges (the so-called “sigma” meson) and short-range mesons (like the omega and the rho) are allowed to contribute to the elastic reaction. Thus, the relevant range of the NN interaction (of a fraction of a fm) is much shorter than the nuclear radius (of several fm). This suggests that the KMT optical potential may be written as

$$V_{\text{KMT}}(\mathbf{r}) \approx \left(\frac{A-1}{A} \right) C(T_{\text{lab}}) \left[\widehat{t}_{0p}(q \equiv 0, T_{\text{lab}}) \rho_p(r) + \widehat{t}_{0n}(q \equiv 0, T_{\text{lab}}) \rho_n(r) \right] . \quad (13)$$

The mismatch in ranges implies that only the forward-angle part of the free NN scattering amplitude is required. Further, as the only remaining radial dependence is contained in the ground-state densities, the optical potential becomes spherically symmetric. This yields the following form for the scattering amplitude:

$$F_0(q, T_{\text{lab}}) \approx \frac{iK}{2\pi} \int_0^\infty b db J_0(qb) (1 - e^{-\chi(b)}) , \quad (14)$$

where J_0 denotes the Bessel function of order $n=0$. As the differential cross section—the sole elastic observable presented in this work—involves the incoherent sum of a large spin-independent amplitude and a small spin-dependent one [see Eq. (4a)], the spin-dependent amplitude will be neglected in the eikonal formalism henceforth.

III. RESULTS

In this section differential cross sections are presented for the elastic scattering of $T_{\text{lab}} = 500$ MeV [28] and $T_{\text{lab}} = 800$ MeV [29] protons from ^{208}Pb . This section is itself divided into three subsections. In the first subsection results are presented according to the formalism outlined in Sec. II C. Having defined the KMT form of the optical potential in Eq. (6), no further approximations are made. Moreover, as the free NN t-matrix is used as input and the ground-state nuclear densities are generated from accurately calibrated models, there is no room left for any adjustable parameters. The free NN t-matrices employed in our calculations are obtained from a meson-exchange model including Delta-isobar degrees of freedom to account for pion-production above the pion threshold. The model is based on the work of Ref. [30] and has recently been revised and updated to fit presently available proton-proton and neutron-proton data up to about 1.2 GeV [31]. Many other choices for the NN t-matrix are possible provided they yield a faithful representation of the experimental data. As we shall see, the KMT results compare very favorably to experimental data at both energies. In the second subsection results are presented in the simpler eikonal approach and are compared against the previously obtained KMT predictions. The goal of this comparison is to use the analytic power of the eikonal approach to elucidate the main features of the data. In particular, we aim to understand the central result of our work: the insensitivity of the differential cross section to our input neutron densities. We reserve the last subsection to address this important point.

A. Non-relativistic KMT Results

The results presented in this section are based on the KMT formalism reviewed in Sec. II C. The differential cross section for the elastic scattering of $T_{\text{lab}} = 500$ MeV and $T_{\text{lab}} = 800$ MeV protons from ^{208}Pb is displayed in Figs. 2 and 3, respectively. The four curves displayed in the figure use the same identical input from the NN sector and differ only in the choice of ground-state densities as described in Sec. II A; the predicted neutron-skin thickness for the various models is indicated in the legend. The experimental data is from Refs. [28] and [29], respectively.

The description of the experimental data—with any one of the four nuclear-structure models—is highly satisfactory. Indeed, the level of success is comparable to that of recent studies that aim to constrain the neutron radius of ^{208}Pb [13, 14, 15]. Further, while theory

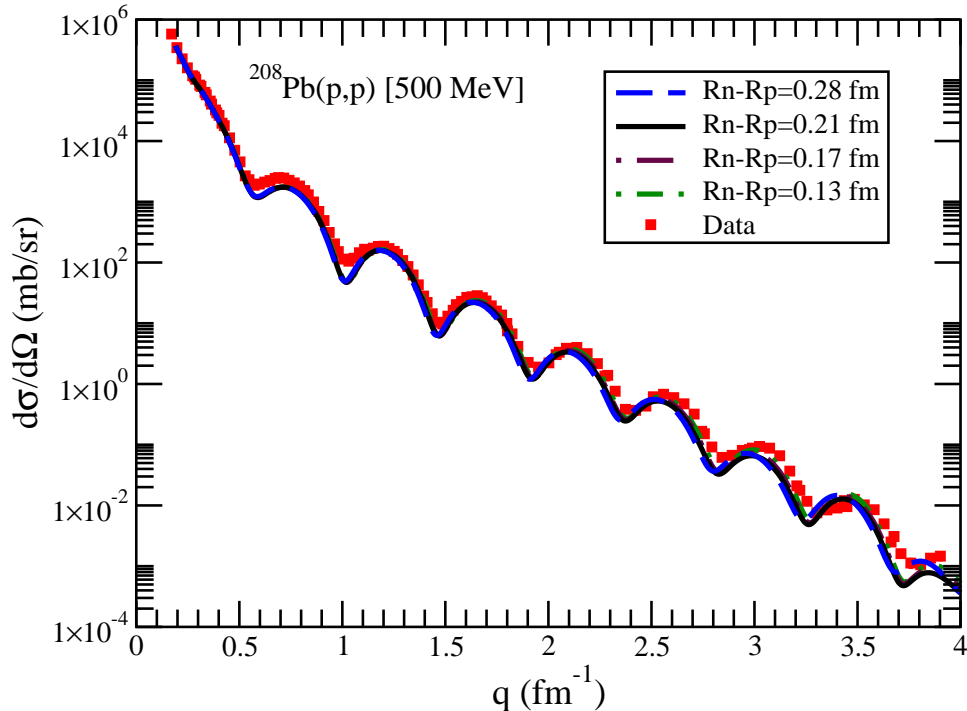


FIG. 2: Elastic scattering cross section of $T_{\text{lab}} = 500$ MeV protons from ^{208}Pb as a function of the momentum transfer to the nucleus. All theoretical models use the KMT optical potential of Eq. (6) with ground-state densities having values for the neutron skin of ^{208}Pb as displayed in the legend. The experimental data is from Ref. [28].

appears to have difficulty in reproducing data at large momentum transfers ($q \gtrsim 3.5$ fm), this happens only after the cross section has dropped by about 8 orders of magnitude. Finally, the observed differences among the four nuclear-structure models is so minute that no clear preference for any of the models emerges. Note that this remains true even if one plots the data in a linear scale, as shown on the inset of Fig. 3.

B. Non-relativistic Eikonal Results

In this section we are willing to sacrifice some degree of accuracy in favor of analytic insight [20, 21]. It is not the aim of this section to replace the highly accurate description achieved above, but rather to complement it with what we hope will be some useful insights. The eikonal calculation reported here differs in three important ways relative to the more accurate KMT approach. First, the mismatch between the small NN range and the large nuclear range enables one to write the optical potential in the form given in Eq. (13). Second, the small spin-dependent component of the scattering amplitude (F_1) is neglected in the description of the incoherent cross section [see Eq. (4a)]. Finally, no long-range Coulomb effects are included. In particular, the omission of Coulomb effects will become clearly distinctive in the diffractive minima of the cross section.

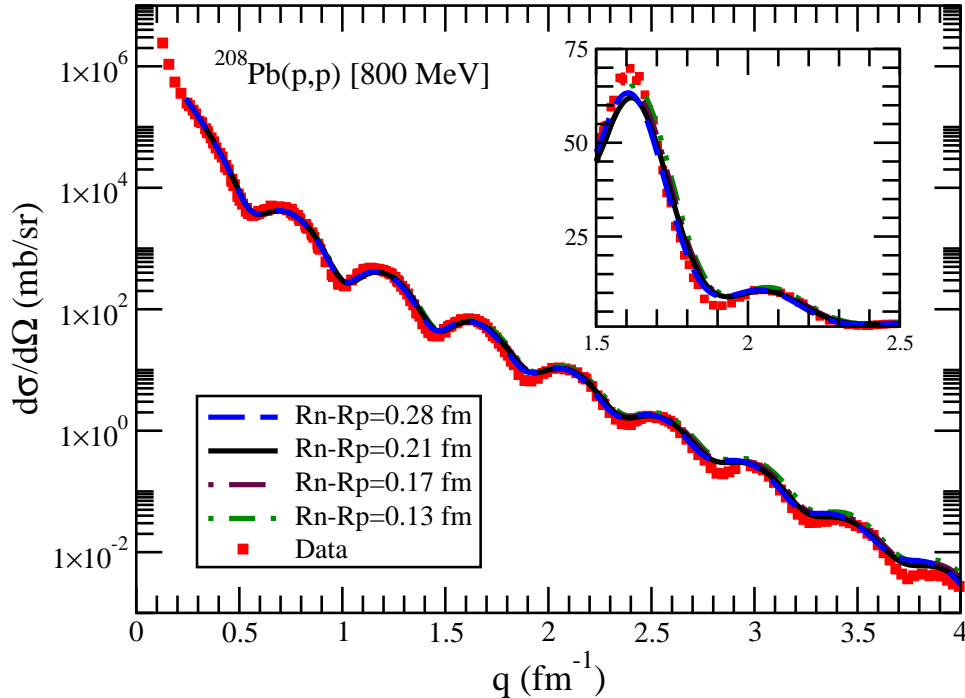


FIG. 3: Elastic scattering cross section of $T_{\text{lab}} = 800$ MeV protons from ^{208}Pb as a function of the momentum transfer to the nucleus. All theoretical models use the KMT optical potential of Eq. (6) with ground-state densities having values for the neutron skin of ^{208}Pb as displayed in the legend. The inset shows the differential cross section on a linear scale over a limited range of momentum transfers. The experimental data is from Ref. [29].

The eikonal results for the differential cross section at $T_{\text{lab}} = 800$ MeV are displayed in Fig. 4, with the various predictions labeled as in Figs. 2 and 3. Evidently, there is a significant loss in quality relative to the full KMT calculation. The cross section is underestimated at small angles, overestimated at large angles, and the predicted minima are too deep. Remarkably, however, the diffractive oscillations and the exponential decay of the cross section are well reproduced. It is the aim of the next section to elucidate these features. Note in closing that as in the KMT case, there is no discernible difference between the models, although some slight separation starts to appear at large momentum transfers ($q \gtrsim 3.5$ fm).

C. Discussion

In this section we resort to analytic insights to elucidate the main features of the elastic cross section, namely, exponentially modulated diffractive oscillations with filled in minima [20, 21]. In comparing the eikonal results to the experimental data (Fig. 4), the most glaring deficiency of the model appears in minima that are too deep. Yet the rapid diffractive oscillations and the exponential falloff are relatively well described. The filling of the minima is strongly sensitive to the underlying NN dynamics, specifically to the real part of the elementary NN t-matrix and the Coulomb interaction. While the former is included

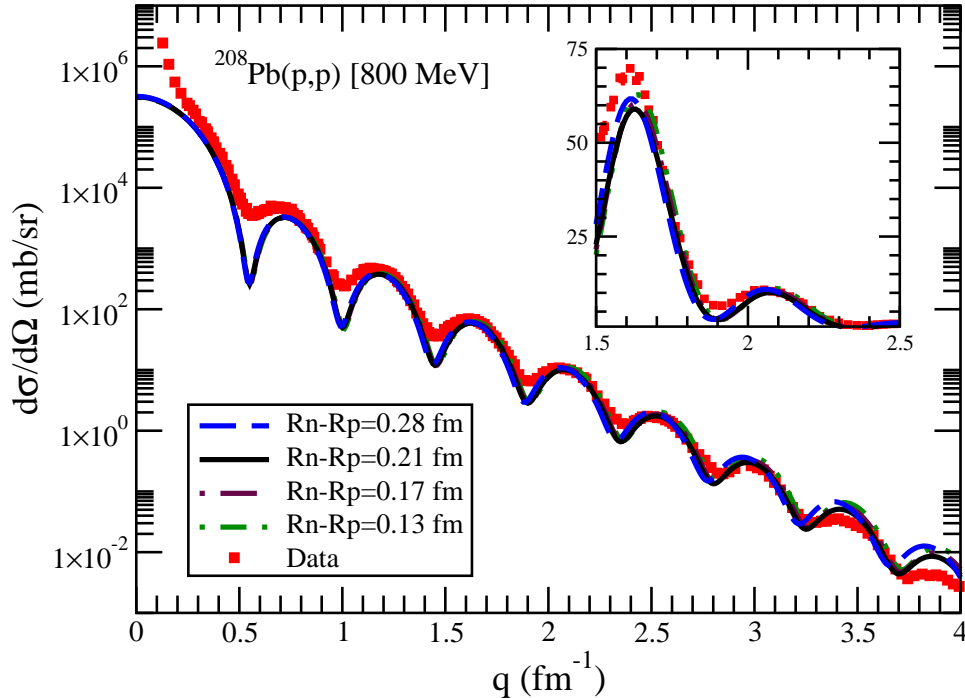


FIG. 4: Elastic scattering cross section of $T_{\text{lab}} = 800$ MeV protons from ^{208}Pb as a function of the momentum transfer to the nucleus. All theoretical models use the simple optical potential of Eq. (13) with ground-state densities having values for the neutron skin of ^{208}Pb as displayed in the legend. The inset shows the differential cross section on a linear scale over a limited range of momentum transfers. The experimental data is from Ref. [29].

in our eikonal calculations [see Eq. 13], the latter is not. Although scattering from a heavy nucleus is strongly sensitive to Coulomb effects, we have decided to neglect them in the eikonal approach (recall, however, that the Coulomb interaction has been fully incorporated in our KMT results [32]). Indeed, rather than adding to the eikonal formalism, we will be removing from it—so we can dissect the various components driving the elastic reaction.

We start from Eq. (13) and rewrite the optical potential in an isoscalar-isovector basis rather than a proton-neutron one. That is,

$$V_{\text{KMT}}(\mathbf{r}) \approx \left(\frac{A-1}{A} \right) C(T_{\text{lab}}) \left[\hat{t}_0(q \equiv 0, T_{\text{lab}}) \rho_0(r) + \hat{t}_1(q \equiv 0, T_{\text{lab}}) \rho_1(r) \right], \quad (15)$$

where $\hat{t}_{0/1} = (\hat{t}_{0p} \pm \hat{t}_{0n})/2$ are the isoscalar/isovector components of the NN t -matrix at forward angles, $\rho_0 = \rho_p + \rho_n$ is the isoscalar (or matter) density, and $\rho_1 = \rho_p - \rho_n$ is the isovector density. There are two factors that make the isovector contribution to the cross section small. First, the isovector density is reduced relative to the isoscalar density by roughly a factor of $(N-Z)/(N+Z) \approx 0.21$. Second, at the energies at which the impulse approximation is valid, the NN amplitude is predominantly isoscalar. To illustrate this point we list in Table III the pp , pn , isoscalar, and isovector scattering amplitudes in the forward direction as a function of the projectile kinetic energy using the NN amplitudes of

T_{lab}	A_{pp}	A_{pn}	A_{isos}	A_{isov}	$ A_{\text{isov}} / A_{\text{isos}} $
400	(+0.1949, 0.3659)	(+0.0874, 0.5441)	(+0.1412, 0.4550)	(+0.0538, -0.0891)	0.2185
500	(+0.0983, 0.4367)	(-0.0364, 0.5733)	(+0.0310, 0.5050)	(+0.0674, -0.0683)	0.1897
600	(+0.0111, 0.5098)	(-0.1446, 0.6051)	(-0.0668, 0.5575)	(+0.0779, -0.0477)	0.1627
700	(-0.0744, 0.5885)	(-0.2434, 0.6430)	(-0.1589, 0.6158)	(+0.0845, -0.0273)	0.1396
800	(-0.1624, 0.6668)	(-0.3385, 0.6819)	(-0.2505, 0.6744)	(+0.0881, -0.0076)	0.1229

TABLE III: Central component of the NN amplitude (in fm) in the forward direction as a function of the laboratory energy (in MeV) of the projectile.

Ref. [31]. These numbers suggest that relative to the dominant isoscalar contribution, the isovector contribution provides at most a 5% correction to the NA scattering amplitude. This point will later be validated by our numerical results (see Fig. 5). Neglecting the isovector contribution yields an eikonal scattering amplitude of the following simple form:

$$F_0(q, T_{\text{lab}}) \approx \frac{iK}{2\pi} \int_0^\infty b db J_0(qb) (1 - e^{-\gamma t(b)}) , \quad (16)$$

where the profile function of Eq. (11) now becomes

$$\chi(b) \approx \gamma t(b) = \frac{\sigma_{\text{tot}}}{2} (1 - ir) \int_{-\infty}^\infty dz \rho_0(r) . \quad (17)$$

Here σ_{tot} is the total NN cross section and r is the ratio of real to imaginary part of the NN forward amplitude. These two equations represent the starting point of the analytic study of Ref. [20].

To separate NN dynamics from nuclear geometry we display in Fig. 5 various calculations that include several levels of approximation. In all these calculations the common denominator is the nuclear density. Only nuclear densities generated from the FSUGold parameter set are included in this illustration. The curve with the very deep minima (short dashes) is generated from Eq. (15) by setting both the isovector term (second term in the expression between brackets) and the real part of the NN amplitude [r in Eq. (17)] to zero. The same exact calculation but with r restored to its physical value yields the curve displayed by the dotted line. As alluded in Refs. [20, 21], we confirm that the real part of the elementary amplitude plays an essential role in filling in the minima. Next we move to the curve represented by the dot-dashed line. This is identical to the one displayed by the black solid line in Fig. 4 and differs from the previous (dotted) one only in that the isovector term has been restored. The imperceptible difference among these two calculations suggests that at the energies considered here the scattering amplitude is strongly dominated by the isoscalar contribution. Next we compare against KMT results. Recall that the KMT scattering amplitude is computed from the optical potential of Eq. (6) without any further approximation. However, in an effort to compare with our eikonal results the Coulomb interaction has been momentarily turned off from the KMT calculation (long dashed line). The difference between this calculation and the previous two eikonal results is minimal. The full KMT calculation with the Coulomb interaction restored (solid line) fills in nicely the minima and provides a faithful representation of the scattering data. Remarkably, the various approximations considered in Fig. 5 affect mostly the minimum-filling of the cross section; the diffractive oscillations and exponential falloff of the cross section are robust and, thus, fairly insensitive to the various approximations.

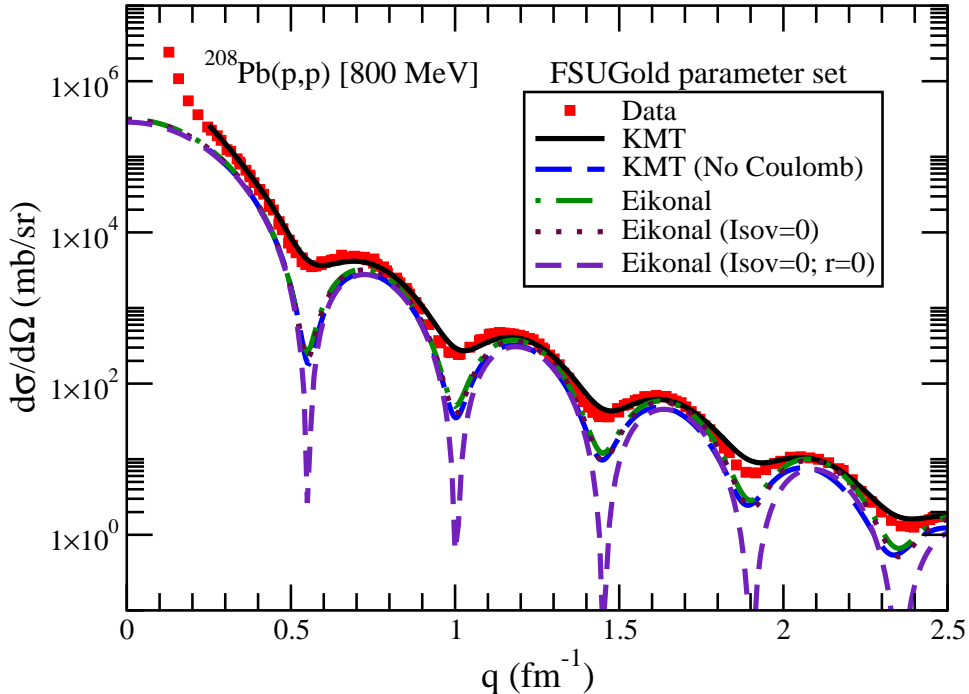


FIG. 5: Elastic scattering cross section of $T_{\text{lab}} = 800$ MeV protons from ^{208}Pb as a function of the momentum transfer to the nucleus. The various theoretical approximations are discussed in the text. All theoretical calculation have been performed using ground-state densities from the FSUGold parameter set. The experimental data is from Ref. [29].

In summary, the eikonal formalism reveals that the main features displayed by the differential cross section are dominated by the nuclear edge, with the radius of the nucleus controlling the diffractive oscillations and the surface thickness the exponential decay. Further, although the diffraction minima are well developed, the minima are filled in—with the filling arising predominantly from the real part of the NN interaction and Coulomb effects. Finally, at the medium energies considered in this work (and necessary for the impulse approximation to be valid) the optical potential is strongly dominated by isoscalar effects.

Within the above context, the insensitivity of the elastic reaction to the nuclear radius should no longer come as a surprise. As argued above, the diffractive oscillations in this medium-energy region are determined by the matter radius R_0 , which is given by

$$R_0 = \sqrt{\frac{Z}{A}R_p^2 + \frac{N}{A}R_n^2} \approx R_p \left(1 + \frac{N}{A} \frac{\Delta R}{R_p}\right) \approx \left[5.46 + 0.23 \left(\frac{\Delta R}{0.21}\right)\right] \text{ fm}. \quad (18)$$

This implies that the more than a factor of two difference in the model dependence of the neutron skin ($\Delta R = 0.13 - 0.28$ fm), gets diluted into a mere 1.5% difference in the matter radius. It is unrealistic to expect that the theoretical uncertainties in this purely hadronic reaction will ever be resolved to the required level of precision.

IV. CONCLUSIONS

We have examined the sensitivity of elastic proton scattering to the neutron radius of ^{208}Pb at projectile energies of $T_{\text{lab}} = 500$ and $T_{\text{lab}} = 800$ MeV. This energy region was selected to minimize the controversial uncertainties in the reaction mechanism inherent to all processes involving strongly-interacting probes. By assuming the validity of the impulse approximation, we exclusively relied on free NN amplitudes that have been determined directly from experimental data. For the nuclear-structure input we relied on two accurately calibrated parameter sets, namely, NL3 [19] and FSUGold [18]. While both sets reproduce binding energies and charge radii of a variety of nuclei, they predict neutron skins in ^{208}Pb that differ considerably: $\Delta R = 0.28$ fm for NL3 and $\Delta R = 0.21$ fm for FSUGold. However, in an effort to expand this range to the region suggested by some recent analyzes [13, 15], the isovector parameters of the FSUGold interaction were tuned to produce two additional parameter sets, one with $\Delta R = 0.17$ fm and the other one with $\Delta R = 0.13$ fm. This tuning was done while maintaining the charge radius of ^{208}Pb within 0.5% of its experimental value.

Calculations were performed in an impulse approximation with a KMT optical potential of the “ $t\rho$ ” form [see Eq. (6)]. The resulting Lippmann-Schwinger equation for the NA amplitude was then solved without resorting to any further approximation. Results for the differential cross section at both energies (500 and 800 MeV) were in good agreement with the experimental data. As important, no clear separation among the nuclear-structure models was observed. This insensitivity of the elastic cross section to the neutron skin of ^{208}Pb represents the main conclusion of this work.

In an effort to understand our numerical results we invoked the eikonal approximation, a formalism that has contributed important insights to our physical understanding [20, 21]. First, we established that in the medium-energy region considered here, the cross section is predominantly sensitive to the matter density. Second, we have verified that while the filling of the diffraction minima arises from a combination of the Coulomb force and the real part of the NN interaction, the diffractive oscillations and its exponential falloff are controlled by the nuclear geometry—with the radius controlling the former and the diffuseness the latter. Since the diffractive oscillations of the cross section are controlled by the matter radius [see Eq. (18)], the large model dependence of the neutron skin got diluted into an unobservable 1.5% difference in the matter radius.

In summary, we find the elastic proton reaction insensitive to the neutron radius of ^{208}Pb . This stands in contradiction to recent results [13, 14, 15]. Thus, we close with a few comments. In Ref. [13] a neutron skin in ^{208}Pb of $\Delta R \simeq 0.17$ fm was suggested from an analysis that included nuclear densities obtained from three different Skyrme interactions and two harmonic-oscillator (HO) parameterizations. While the data can easily discriminate between the Skyrme and HO models, distinguishing among the three Skyrme interactions becomes possible only at large angles for the largest energy considered ($T_{\text{lab}} = 200$ MeV). Unfortunately, in the large-angle region where the model dependence is the largest, there also appears to be a significant discrepancy between theory and experiment. In the relativistic approach of Ref. [14] an optimal set of neutron-density parameters is obtained by means of a global fit to a large body of scattering observables. From this analysis the neutron skin of ^{208}Pb was constrained to the range $\Delta R \sim 0.083 - 0.111$ fm. However, what is sorely missing from these two analyzes is a discussion on how much will the description of the differential cross section suffer by including other realistic neutron densities having similar surface properties but different neutron radii. For example, could the non-relativistic work

of Ref. [13] still provide a good description of the scattering data by using neutron densities with the smaller neutron radius of Ref. [14]?

A partial answer—in the affirmative—to this question has been provided in Ref. [15]. By using the SkM* Skyrme interaction of Ref. [13] together with a realistic RPA interaction, an excellent description of the differential cross section for the elastic scattering of $T_{\text{lab}} = 121$ MeV protons from ^{208}Pb was obtained. Thus, the range of acceptable values of the neutron skin of ^{208}Pb got extended to the region $\Delta R \simeq 0.13 - 0.17$ fm. In this contribution we have extended the range even further: to $\Delta R \simeq 0.13 - 0.28$ fm. Note, however, that we were unable to rule out neutron skins outside this range.

Proton-induced reactions have evolved to a point that cross section measurements over ten orders of magnitude are now routine. Even so, it is unrealistic to expect them to evolve into precision tools, mainly because of the large uncertainties inherent in any theoretical description of strongly interacting reactions. Still, the decisive role that these reactions will play in our understanding of novel properties of exotic nuclei is without question. Yet for a clean and model independent extraction of the neutron radius of ^{208}Pb we must resort to electroweak probes. At present, the Parity Radius Experiment at the Jefferson Laboratory appears as the only alternative for providing a unique experimental constraint on the thickness of the neutron skin of a heavy nucleus.

Acknowledgments

We thank Brandon van der Ventel for many useful discussions and Charlotte Elster for providing us with the NN -potential code and for a careful reading of the manuscript. S.P.W. gratefully acknowledges Kirby Kemper and the Physics Department at Florida State University for their hospitality during his sabbatical leave. This work was supported in part by DOE grant DE-FG05-92ER40750.

-
- [1] G. Fricke, C. Bernhardt, K. Heilig, L. A. Schaller, L. Schellenberg, E. B. Shera, and C. W. de Jager, *Atom. Data and Nucl. Data Tables* **60**, 177 (1995).
- [2] R. Hofstadter, H. R. Fechter, and J. A. McIntyre, *Phys. Rev.* **91**, 422 (1953).
- [3] L. Ray and G. W. Hoffmann, *Phys. Rev. C* **31**, 538 (1985).
- [4] L. Ray, G. W. Hoffmann, and W. R. Coker, *Phys. Rep.* **212**, 223 (1992).
- [5] C. J. Horowitz, S. J. Pollock, P. A. Souder, and R. Michaels, *Phys. Rev. C* **63**, 025501 (2001).
- [6] R. Michaels, P. A. Souder, and G. M. Urciuoli, *Neutron skin of lead through parity violating electron scattering* (2002).
- [7] B. A. Brown, *Phys. Rev. Lett.* **85**, 5296 (2000).
- [8] A. W. Steiner, M. Prakash, J. M. Lattimer, and P. J. Ellis, *Phys. Rep.* **411**, 325 (2005).
- [9] C. J. Horowitz and J. Piekarewicz, *Phys. Rev. Lett.* **86**, 5647 (2001).
- [10] C. J. Horowitz and J. Piekarewicz, *Phys. Rev. C* **64**, 062802(R) (2001).
- [11] C. J. Horowitz and J. Piekarewicz, *Phys. Rev. C* **66**, 055803 (2002).
- [12] J. Carriere, C. J. Horowitz, and J. Piekarewicz, *ApJ*. **593**, 463 (2003).
- [13] S. Karataglidis, K. Amos, B. A. Brown, and P. K. Deb, *Phys. Rev. C* **65**, 044306 (2002).
- [14] B. C. Clark, L. J. Kerr, and S. Hama, *Phys. Rev. C* **67**, 054605 (2003).
- [15] M. Dupuis, S. Karataglidis, E. Bauge, J.-P. Delaroche, and D. Gogny (2005), [nucl-th/0506077](#).
- [16] K. Amos, P. J. Dortmans, H. V. Geramb, S. Karataglidis, and J. Raynal, in *Advances in Nuclear Physics, Vol. 25*, edited by J. W. Negele and E. Vogt (Plenum Publishers, New York, 2000), and references within.
- [17] J. Piekarewicz, *Phys. Rev. C* **69**, 041301 (2004).
- [18] B. G. Todd-Rutel and J. Piekarewicz (2005), [nucl-th/0504034](#).
- [19] G. A. Lalazissis, J. Konig, and P. Ring, *Phys. Rev. C* **55**, 540 (1997).
- [20] R. D. Amado, J. P. Dedonder, and F. Lenz, *Phys. Rev. C* **21**, 647 (1980).
- [21] R. D. Amado, in *Advances in Nuclear Physics, Vol. 15*, edited by J. W. Negele and E. Vogt (Plenum Publishers, New York, 1985).
- [22] H. Müller and B. D. Serot, *Nucl. Phys.* **A606**, 508 (1996).
- [23] J. D. Walecka, *Annals Phys.* **83**, 491 (1974).
- [24] C. Horowitz and B. D. Serot, *Nucl. Phys.* **A368**, 503 (1981).
- [25] B. G. Todd and J. Piekarewicz, *Phys. Rev. C* **67**, 044317 (2003).
- [26] A. K. Kerman, H. McManus, and R. M. Thaler, *Annals Phys.* **8**, 551 (1959).
- [27] A. Picklesimer, P. C. Tandy, R. M. Thaler, and D. H. Wolfe, *Phys. Rev. C* **30**, 1861 (1984).
- [28] D. A. Hutcheon *et al.*, *Nucl. Phys. A* **483**, 429 (1988).
- [29] G. W. Hoffmann *et al.*, *Phys. Rev. C* **21**, 1488 (1980).
- [30] C. Elster, K. Holinde, D. Schütte, and R. Machleidt, *Phys. Rev. C* **38**, 1828 (1988).
- [31] A. Schwick, Ph.D. thesis, University of Bonn (2004), to be published.
- [32] C. R. Chinn, C. Elster, and R. M. Thaler, *Phys. Rev. C* **44**, 1569 (1991).